

Microstructural evolution and enhanced properties by multi-directional forging of 6201 aluminum alloy

Shun Zhang^{1,2}, Guangzong Zhang^{1,2} , Da Teng^{1,2}, Changfeng Wang^{1,2}, Xuan Zhang^{1,2}, Renguo Guan^{1,2}

¹Dalian Jiaotong University, Key Laboratory of Near-Net Forming of Light Metals of Liaoning Province. Dalian, 116028, China.

²Dalian Jiaotong University, Ministry of Education, Engineering Research Center of Continuous Extrusion. Dalian, 116028, China.

e-mail: gzzhang@djtu.edu.cn, 15161921005@163.com, dateng120812@163.com, 442372206@qq.com, chfwang@djtu.edu.cn, guanrenguo@sina.cn

ABSTRACT

In this work, the microstructure evolution and mechanical properties of 6201 aluminum alloy during multi-directional forging (MDF) and solution-aging were systematically studied. In the MDF process, the deformation of 6201 aluminum alloy was not uniform, and the increase of forging passes can effectively improve the inhomogeneity. With the increase of forging passes, the alloy changed from dynamic recovery to dynamic recrystallization, the grains in the center were refined obviously, and the anisotropy of microstructure was eliminated. After 9 passes of MDF followed by the solution-aging, the re-dissolution and re-precipitation behavior of the second phases significantly improved the mechanical properties of the alloy. The tensile strength, yield strength, elongation and conductivity of the alloy were 257 MPa, 139 MPa, 16.1%, 51.6% IACS, respectively, 55.8%, 73.8%, 3.4% and 10.5% higher than that of the as-cast alloy. At the same time, the average grain size of the alloy was decreased to 133 μm , 50.9% lower than that of the initial one.

Keywords: 6201 aluminum alloy; Multi-directional forging; Uniformity; Properties.

1. INTRODUCTION

Severe plastic deformation (SPD) is an effective method to refine grain and improve the mechanical properties of materials. Equal Channel Angular Pressing (ECAP) [1–3], High Pressure Torsion (HPT) [4, 5], Cyclic Extrusion Compression (CEC) [6], Accumulative Roll Bonding (ARB) [7], Multi-Directional Forging (MDF) [8] and so on are all existing SPD technologies. The ultrafine grain structure produced by SPD process facilitates the excellent performance. MDF has the advantages of simple structure and low cost, which has the potential to produce the large-volume products. Through the MDF, the material is continuously compressed and elongated with the axial change of the applied load, and the grain refinement and better performance are achieved by the repeated deformation.

In past years, the applications of MDF in non-ferrous metals have been carried out. ZHANG *et al.* [9] prepared large-scale industrial samples of AZ80 alloy with a size of $100 \times 100 \times 140 \text{ mm}^3$ by two-step MDF process and artificial aging process. After MDF, the yield strength (YS), ultimate tensile strength (UTS) and elongation (EL) of AZ80 alloy increased to 303 MPa, 397 MPa and 11.2%, respectively. After T5 treatment, the YS and UTS further increased to 343 MPa and 430 MPa. While the sample maintained a high EL of 11.4%. WANG *et al.* [10] forged 7A85 aluminum alloy in multiple directions at 470 °C through three different forging processes. It was found that cumulative deformation resulted in the serious lattice distortion, vacancies and dislocations etc., thereby improving the performance of the alloy. The above experiments are mostly hot deformation processes, involving dynamic recovery (DRV) and dynamic recrystallization (DRX). EBRAHIMI and SHAFIEI [11] discussed the basic concepts of thermal deformation and dynamic recovery, including factors that affect dynamic recrystallization and dynamic recrystallization processes, as well as related tissue evolution. Simultaneously, a large number of experimental and mathematical models such as constitutive equations were organized, and their accuracy and limitations were evaluated. Similarly, during MDF of as cast 7475 alloy by SITDIKOV *et al.* [12], a large number of recrystallized grains with high angle grain boundaries were formed, and the grains were effectively refined. The results showed that cumulative deformation is an important factor

affecting grain size. RAO *et al.* [13] studied the evolution of microstructure and mechanical properties of 6061 aluminum alloy during MDF in liquid nitrogen. When the strain accumulated to 5.4, the microstructure texture was mainly equiaxed subgrains with large angle grain boundaries, and the grain size was about 250 nm. The Vickers hardness of the material increased from 50 Hv to 115 Hv, combined with the increasing tensile strength from 180 MPa to 388 MPa. AOBA *et al.* [14] systematically studied the microstructure evolution and mechanical properties of 6000 series aluminum alloys during MDF and artificial aging. With the increase of cumulative strain, the strength increases gradually. The sample aged at 120 °C for 100 ks showed a good balance of mechanical properties, i.e., UTS of 313 MPa, YS of 288 MPa, and EL of 18.9%. MIKHAYLOVSKAYA *et al.* [15] found that, in the isothermal multi-directional forging process, the Al_3Mg_2 phase in Al-Mg based alloys was involved in the PSN effect. It led to a uniform recrystallized grain structure of Al-Mg based alloys. The fine and uniform microstructure improved the yield strength. MOGHANAKI *et al.* [16] found that, there were a large number of intermetallic compound particles during non isothermal annealing of multi-directional forging solution treated AA2024 alloy, and the Fe rich particles were preferred sites for recrystallization nucleation. At the same time, the PSN effect was related to the Zener pinning effect of Al_2CuMg fine particles. During non isothermal annealing in the range of 380–450 °C, increased temperature would promote the PSN. Similarly, in the study of the effect of cumulative strain on the microstructure and properties of multi-directional forged 2A14 aluminum alloy, WANG *et al.* [17] found that the high-temperature precipitate of Al_2Cu phase and the dynamic precipitation during aging were beneficial for grain refinement. Researches have fully demonstrated that, MDF can refine grains and improve the mechanical properties of alloys in the field of non-ferrous metals. However, less researches focus on the anisotropy of alloys and the uniformity of alloys in center and edges under different processes. Though, some scholars have conducted MDF researches on 6xxx aluminum alloys, alloys with high strength and high conductivity have rarely been developed.

In the 6xxx aluminum alloys, the 6201 alloy owes the high strength and a relatively high conductivity. In this work, experimental research and theoretical analysis were carried out to change the forging pass and heat treatment process. The effects of forging passes and heat treatment on the microstructure and properties of 6201 aluminum alloy were analyzed. The parameters were optimized, and a large-scale industrial sample with excellent properties was developed, which provided a reference for future research.

2. MATERIALS AND METHODS

6201 commercial aluminum alloy was used, and the chemical compositions are shown in Table 1. Figure 1 shows the schematic diagram of MDF, and the ingot with a size of $110 \times 110 \times 160 \text{ mm}^3$ was prepared. After the heat treatment at 500 °C for 1 hour in a resistance furnace, the ingot was subjected to different passes of MDF. The deformation of each pass is ~40%. The axis of the forging is parallel to the vertical direction of the “X”, “Y”, and “Z” planes, respectively. Combined with the alloy microstructure, the sample after 9 passes was subjected to solid solution treatment at 535 °C for 1 hour and the aging at 173 °C for 8 hours.

Figure 2 shows the position and the dimensions of the samples for microstructure observation and mechanical property test. Among them, the size of the OM sample used for observation was $10 \times 10 \times 12 \text{ mm}^3$. The size of the stretching rod was shown in the figure. The size of tested conductive sample was $8 \times \Phi 20$, and that of the EBSD sample was $8 \times 8 \times 2.5 \text{ mm}^3$. The microstructure of the sample was observed using an optical microscope (OM, Olympus DSX500, Japan), and scanning electron microscope (SEM, Zeiss Sigma 300, Germany) with electron backscatter diffraction (EBSD, Oxford Nordly max3, UK). Furthermore, the collection range of EBSD sample was selected as $1600 \times 1600 \mu\text{m}^2$, the step size was 2 μm . EBSD analysis was performed using the orientation microscopy software HKL-Channel-5 software. The second phases were detected using an X-ray diffractometer (XRD, PANalytical X Pertpro, Netherlands). The tensile test was carried out at room temperature using an electronic universal testing machine (AG-XPLUS100KN, Japan). The conductivity was measured by eddy current conductivity meter (PZ 60A, China). The mean value of the conductivity was measured 8 times to ensure the accuracy. All samples used for testing were polished with 400 #–5000 # sandpaper to ensure a smooth and even surface. The OM samples were ground and etched in 10% hydrofluoric acid solution after mechanical polishing with diamond gypsum, and the samples used for EBSD analysis were mechanically polished with diamond gypsum and argon ion polished after grinding. The ion polishing process was conducted at 6 kV for 50 minutes.

Table 1: Chemical compositions of the experimental alloy (wt.%).

CHEMICAL COMPOSITION	Fe	Si	Mn	Cr	Cu	B	Al	Zn	Mg
Minimum value	–	0.5	–	–	–	–	97.28	–	0.6
Maximum value	0.5	0.9	0.03	0.03	0.1	0.06	98.9	0.1	0.9

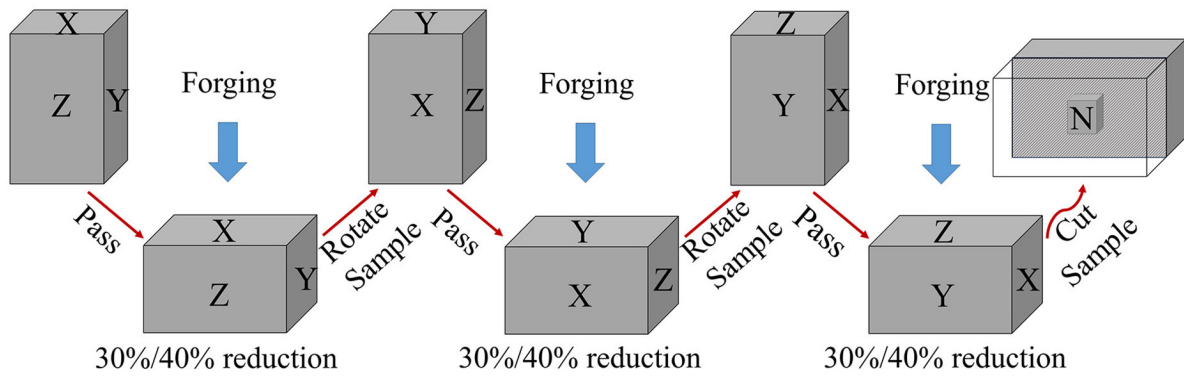


Figure 1: Schematic diagram of MDF.

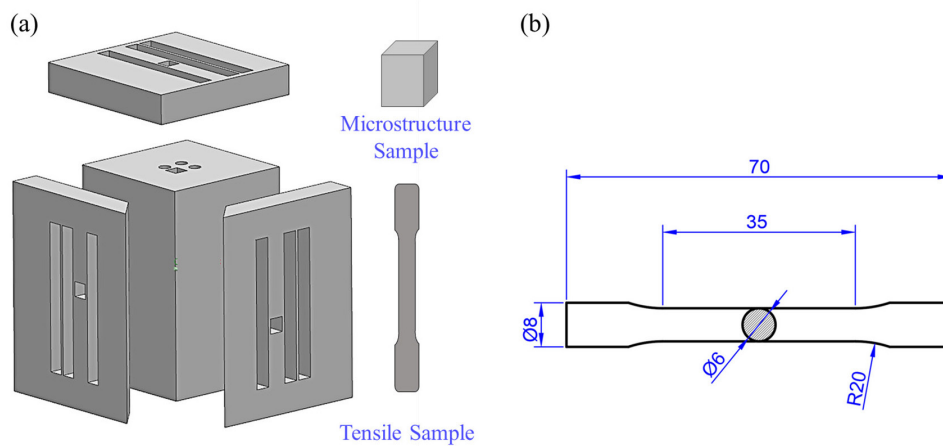


Figure 2: Position (a) and the dimensions (b) of the samples for microstructure observation and mechanical property test.

3. RESULTS AND DISCUSSION

3.1. Microstructure evolution during MDF

Figure 3a-d show the microstructure of the alloys in X, Y, Z and N zones at different passes. As shown in Figure 3(a1)–(d1), the microstructure in X zone retains the as-cast coarse equiaxed crystal morphology at 3 passes, and the grain size is determined as $\sim 240 \mu\text{m}$. Simultaneously, that of Y, Z and N regions is $238 \mu\text{m}$, $243 \mu\text{m}$ and $208 \mu\text{m}$, respectively. Thus, the grains in N zone are more prone to deformed when the cylinder is upsetting. In addition, due to the deformation of each region during MDF is not accurately controlled, the grain sizes are different, some of them tend to be elongated in a certain direction, characterized by the fibrous structure. In addition, with the increase of passes, the grain sizes in different regions decrease, and the grain sizes of X, Y and Z zones are closer. As shown in Figure 3(a3)–(d3), the grain sizes of the X, Y and Z regions are about $120 \mu\text{m}$. During the MDF, the grain size of the N zone keeps the smallest, which is $\sim 118 \mu\text{m}$ at 9 passes. Thus, the MDF can refine the grain size and reduce the inhomogeneity of the sample. With the increase of deformation passes, the degree of dynamic recrystallization gradually increases, and the grains become finer. However, after 12 passes, the grain size of N region slightly increases, $\sim 121 \mu\text{m}$, which should be attributed to the thermal effect during the continuous deformation, facilitating the growth of the recrystallized grains. Therefore, further increasing the deformation passes has no significant refinement of the alloy.

During the MDF, the single-pass forging strain rate is high and the deformation time is short. The deformation zone initiates from some grains, and the recrystallized grains are formed near the grain boundary. With the continuous change of the load direction, the interlaced deformation zones are formed inside the grains, and the original as-cast grains are broken along the path of the deformation zone. The serious lattice distortion around the deformation zone induces more nucleation conditions, so as to achieve the grain refinement. As reported by WANG *et al.* [10], with the increase of cumulative deformation, the recrystallization difference between the center and edge decrease, facilitating to form a more uniform structure.

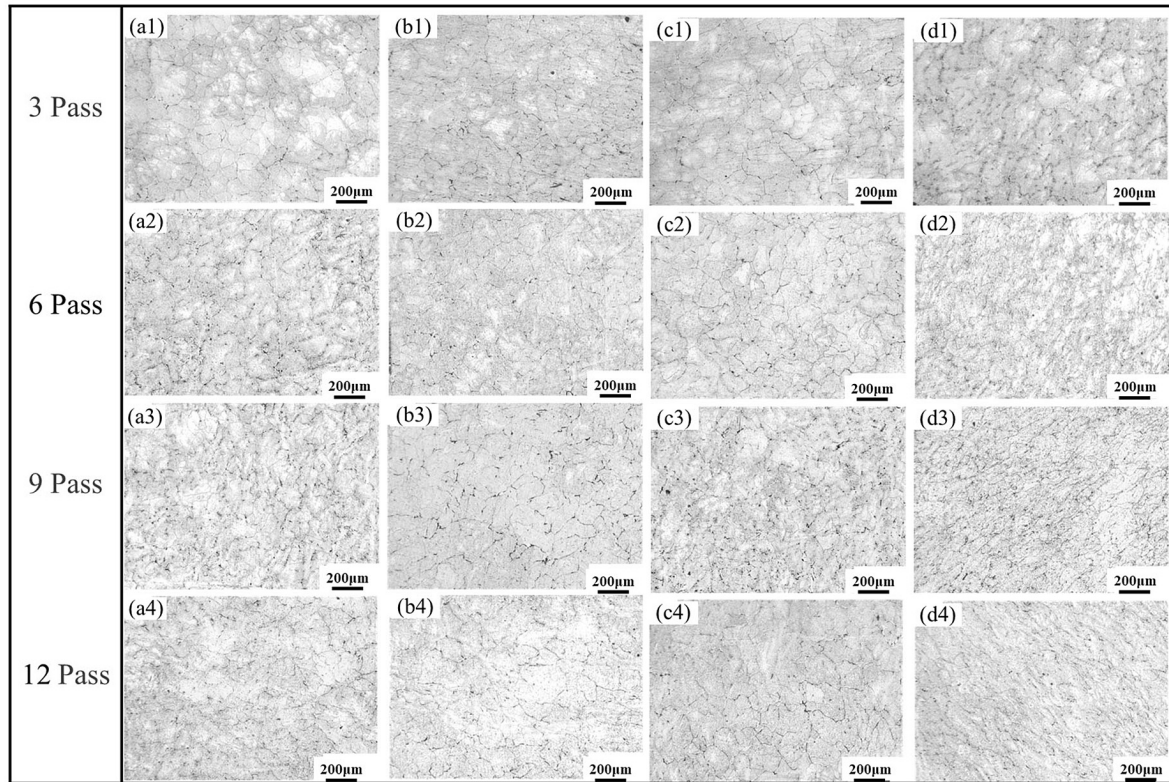


Figure 3: OM images of each region of 6201 aluminum alloy at different passes of MDF. 3 passes (a1)–(d1), 6 passes (a2)–(d2), 9 passes (a3)–(d3), 12 passes (a4)–(d4).

3.2. Texture development during MDF

Aluminum alloy belongs to polycrystalline material, which has the characteristics of anisotropy of polycrystalline material. Plastic deformation induces the grains to form textures. Since the formation and evolution of textures directly affect the alloy properties, regulating texture is an effective way to strengthen the properties of the alloy [18]. In order to reveal the effect of MDF on the anisotropy, the textures of the X, Y, Z and N regions of the alloy after 9 passes of MDF were tested. The results are shown in Figure 4. From Figure 4a-d, the red, blue and green represent $\langle 001 \rangle$, $\langle 111 \rangle$ and $\langle 101 \rangle$ crystallographic directions. It could be found that, the texture is mainly composed of grains with higher strength oriented $\langle 001 \rangle$ in red and $\langle 101 \rangle$ in green, and the microstructure differences among the four regions of the alloy can be neglected at 9 passes. As reported by CHEN *et al.* [19], under the large deformation, $\langle 101 \rangle$ texture is unstable and will be transformed into $\langle 001 \rangle$ and $\langle 111 \rangle$ orientations. On the contrary, under the small deformation, $\langle 111 \rangle$ texture is unstable and will be transformed into $\langle 101 \rangle$ and $\langle 001 \rangle$ orientations. For the X, Z and N regions, the grain orientation is mainly $\langle 001 \rangle$, while for the Y region, it is $\langle 001 \rangle$ and $\langle 101 \rangle$. This indicates the differences in each region during the large deformation of MDF. In addition, the texture strengths of X, Y and Z zones are close, which are 5.24, 5.59 and 5.04, respectively. While the texture intensity of the N region is the highest, reaching 6.93, which signifies the strong texture and the weakened anisotropy. As the easy deformation zone, the N zone has smallest grain size with the highest texture strength, which indicates the best mechanical properties. However, as shown in Figure 4e and f, the tensile strengths of X, Y, Z, and N zones are 212, 215, 208, and 223 MPa, respectively, with small differences in performance of each region. WANG *et al.* [17] reached a similar conclusion after conducting multi-directional forging on 2A14 aluminum alloy. They measured the hardness of different regions and found that there was little difference in hardness. Combined with the grain size change in Figure 3, the negligible difference in texture strength shows the uniform microstructure in different regions after MDF. Therefore, the N region of each forging is adopted to compare in followings.

The effect of deformation on grain refinement during MDF of aluminum alloy is mainly reflected in two aspects: Firstly, the coarse grain is broken under the action of deformation. The range of deformation zone is expanded, and the effective area of recrystallized grain nucleation per unit volume is increased, which is conducive to form the recrystallized grains and refine the grains. Secondly, the misorientation of the

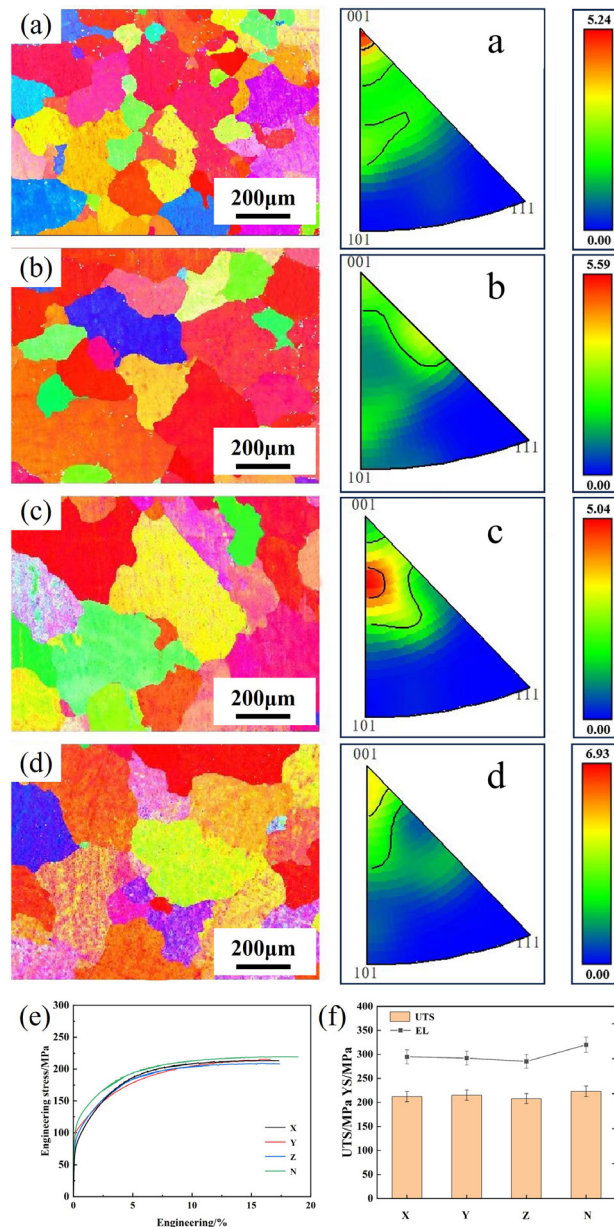


Figure 4: Orientation image and inverse pole figure of the alloys in X(a), Y(b), Z(c) and N(d) zone at 9 passes, tensile properties (e) and (f).

deformation band gradually increases, resulting in the adjustment of the orientation of each part of the coarse grains and affecting the texture strength.

3.3. Second phases evolution during MDF

For each alloy, the second phases in the microstructure at different passes and positions are the same. As shown in Figure 5, the alloy consists of three phases: α -Al, Mg_2Si and $Al_{0.5}Fe_3Si_{0.5}$.

Figure 6 shows the SEM and EDS results of the alloys in N zone at 9 passes. The alloy is mainly composed of α -Al matrix defined as point A, the long flake white phase $Al_{0.5}Fe_3Si_{0.5}$ defined as point B and the spherical black phase Mg_2Si defined as point C. According to the relevant research, Mg_2Si is an intermetallic compound, which plays a key role in improving the alloy strength. While $Al_{0.5}Fe_3Si_{0.5}$ is a compound produced by chemical reaction, which is unfavorable to the mechanical properties of the alloy in as-cast state [20–24].

Figure 7 shows the SEM images of the alloys in N zone at different MDF passes. As shown in Figure 7a and b, a large number of Mg_2Si phases exist in the matrix at 3 passes, and some of them are attached to $Al_{0.5}Fe_3Si_{0.5}$, which presents as the large fragment. From Figure 7c and d, the Mg_2Si phase is reduced, and the $Al_{0.5}Fe_3Si_{0.5}$

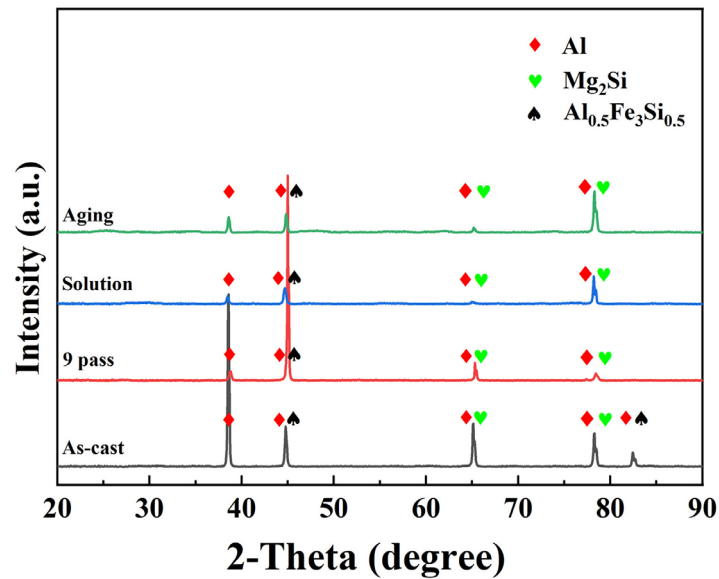


Figure 5: XRD patterns of the alloys in N zone at different states.

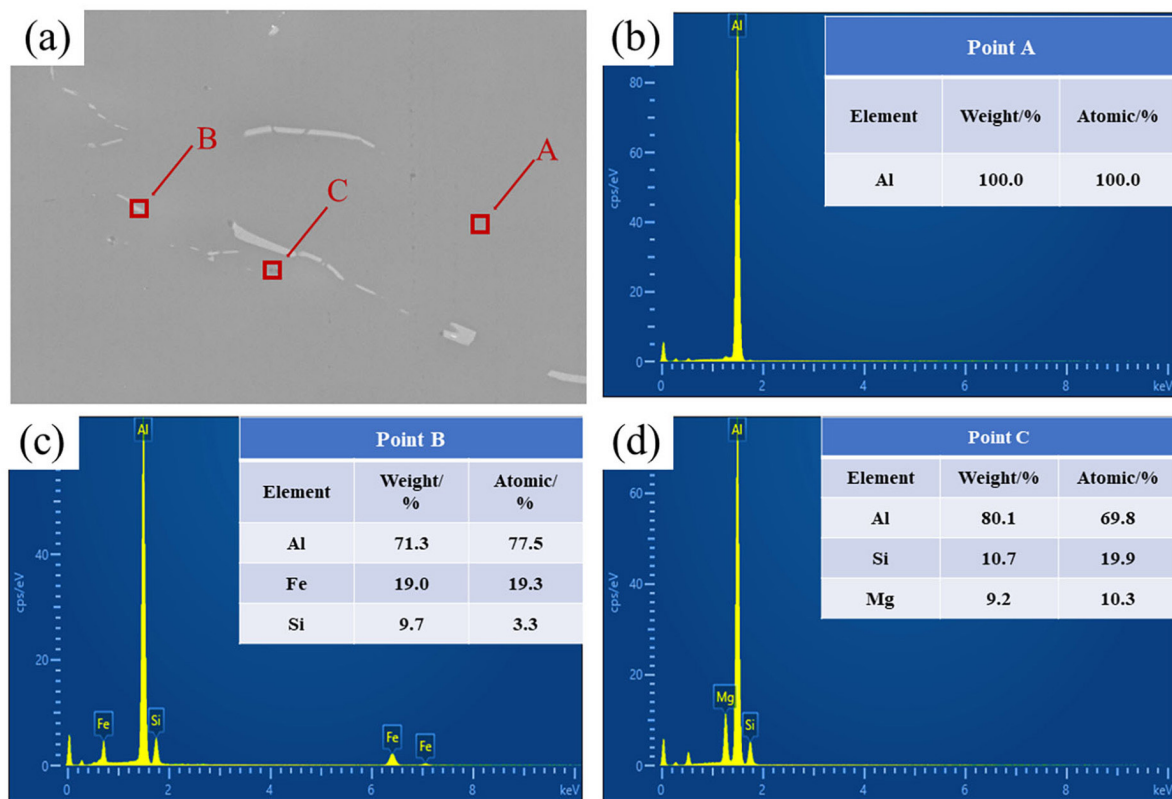


Figure 6: SEM images of the alloys in N zone at 9 passes (a) and the EDS results of points A (b), B (c) and C (d).

fragments become dispersed. Further increasing the pass to 9, as shown in Figure 7e and f, Mg_2Si phases disappear, and the size of $Al_{0.5}Fe_3Si_{0.5}$ phases is reduced to 0.2–5 μm . This phenomenon is called severe plastic deformation-induced second-phase re-dissolution [25].

Furthermore, as the deformation proceeds, the heat is accumulated and the lattice distortion is increased, which not only causes the vacancies, dislocations and other defects, but promotes the dissolution of second

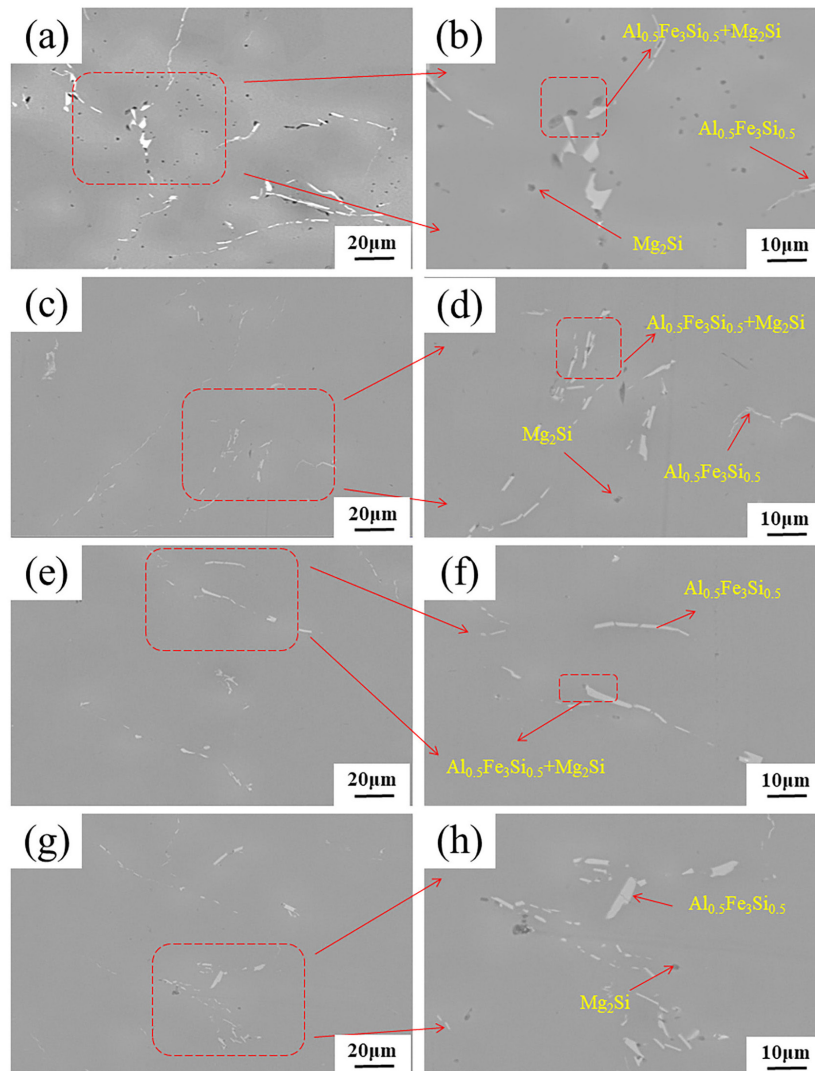


Figure 7: SEM images of the alloys in N zone at different MDF passes. 3 passes (a) and (b), 6 passes (c) and (d), 9 passes (e) and (f), 12 passes (g) and (h).

phase. As shown in Figure 7g and h, a small amount of Mg_2Si phases precipitate at 12 passes, accompanied with the larger $Al_{0.5}Fe_3Si_{0.5}$ fragments of $\sim 1\text{--}10\ \mu m$, which should be attributed to the thermal effect under the continuous deformation. For the re-dissolution of the second phase induced by severe plastic deformation, the following viewpoints are considered. Firstly, the strong plastic deformation leads to an increase in the surface energy of the second phase, thereby promoting its re-dissolution [26]. Secondly, the fine grain size will lead to the high solubility around it, thus inducing the second phase to dissolve [27]. The mechanism of the second phase re-dissolution is further studied.

In view of the symbiosis phenomenon of Mg_2Si and $Al_{0.5}Fe_3Si_{0.5}$ phases, the N zone of the alloy at 9 passes was selected for analysis. The microstructure of the composite phase is shown in Figure 8. The gray $Al_{0.5}Fe_3Si_{0.5}$ occupies most of the area, and the black Mg_2Si phase distributes around it. It is speculated that, when the $Al_{0.5}Fe_3Si_{0.5}$ phase is generated, the excess Mg atoms will be excluded, resulting in the enrichment of Mg elements around. This promotes the precipitation of Mg_2Si . From the mapping in Figure 8b-d, a large amount of Mg element enriches around the Si and Fe elements, demonstrating the relationship between Mg_2Si and $Al_{0.5}Fe_3Si_{0.5}$ phases [28].

3.4. Heat treatment after MDF

The samples at 9 passes were subjected to solution treatment for 1h and aging for 8h. The average grain sizes of these samples are shown in Table 2. Compared with the original as-cast alloy, the average grain size of the alloy at 9 passes, after solution treatment and aging, decreases by 56.5%, 52.6% and 50.9%, respectively.

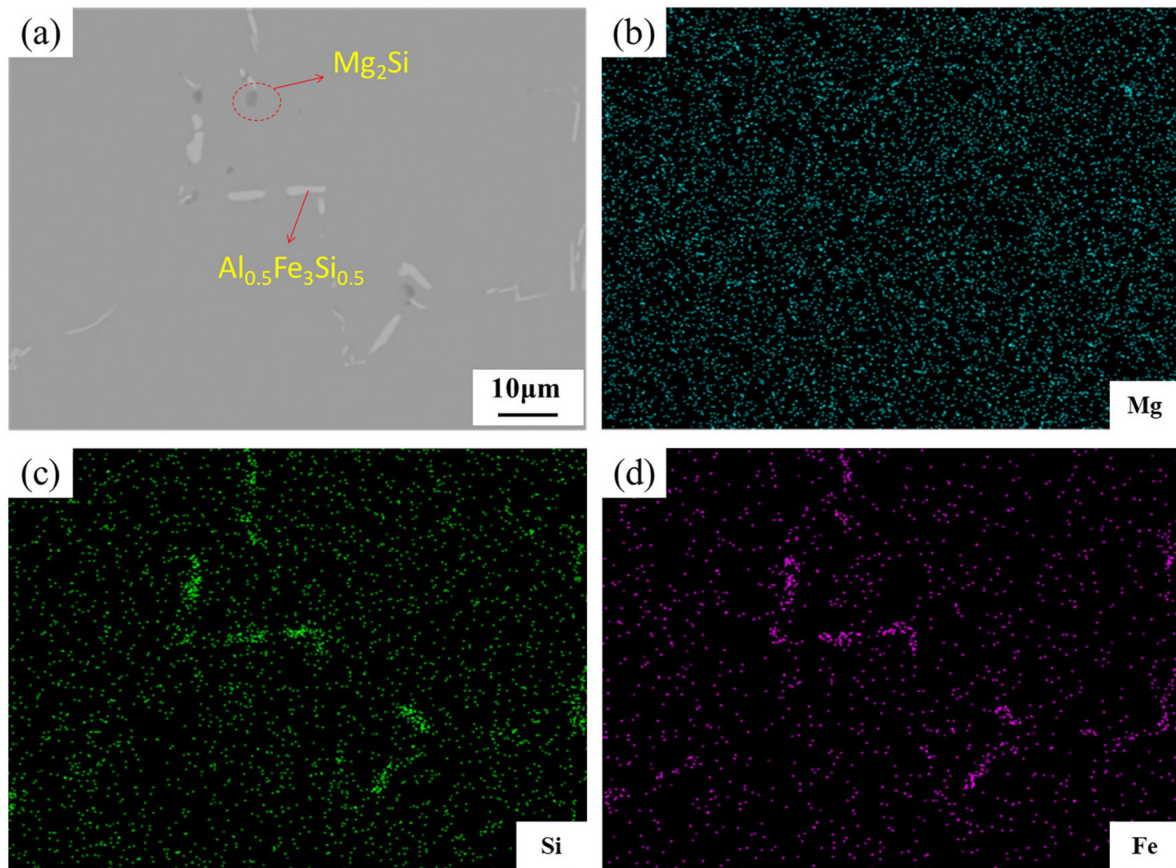


Figure 8: SEM images of the alloy in N zone (a), and mapping of element Mg (b), Si (c), and Fe (d).

Table 2: Changes in grain size during heat treatment.

STATE	AVERAGE GRAIN (mm)	SIZE VARIATION (%)
As-cast structure	271	0
9 passes	118	56.5
Solution treatment	128	52.6
Aging	133	50.9

As indicated in Figure 5, the XRD patterns of the alloys in N zone are composed of α -Al, Mg_2Si phase and $Al_{0.5}Fe_3Si_{0.5}$ phase. In addition, with the progress of forging and heat treatment, the intensity of the diffraction peaks changes significantly. During forging and solution, a large amount of Mg_2Si dissolves in the matrix, then precipitates again during aging process. Throughout the whole process, the change in the peak intensity of $Al_{0.5}Fe_3Si_{0.5}$ can be negligible.

Figure 9 shows the SEM images of the alloys in N zone at different states. As shown in Figure 9a and b, the block like $Al_{0.5}Fe_3Si_{0.5}$ phase exists in the matrix of the as-cast alloy. From Figure 9c and d, the size and the number of $Al_{0.5}Fe_3Si_{0.5}$ phase after 9 passes of MDF is significantly reduced, and the distribution is more dispersed. Simultaneously, a large amount of Mg_2Si phases disappear, which should be attributed to the effect of severe plastic deformation. From Figure 9e and f, after 9 passes of MDF and solution treatment, the size of $Al_{0.5}Fe_3Si_{0.5}$ phase decreases, and Mg_2Si phase further disappears. Only a small amount of Mg_2Si phases with a size of less than $1\mu m$ were observed on the broken $Al_{0.5}Fe_3Si_{0.5}$. After aging, as shown in Figure 9g and h, the size of the second phases become larger. The size of Mg_2Si phase is about $2-3\mu m$. And it's attached to the $Al_{0.5}Fe_3Si_{0.5}$ phase, which should be originated from the lattice matching relationship between the two phases, as reported by GU *et al.* [29].

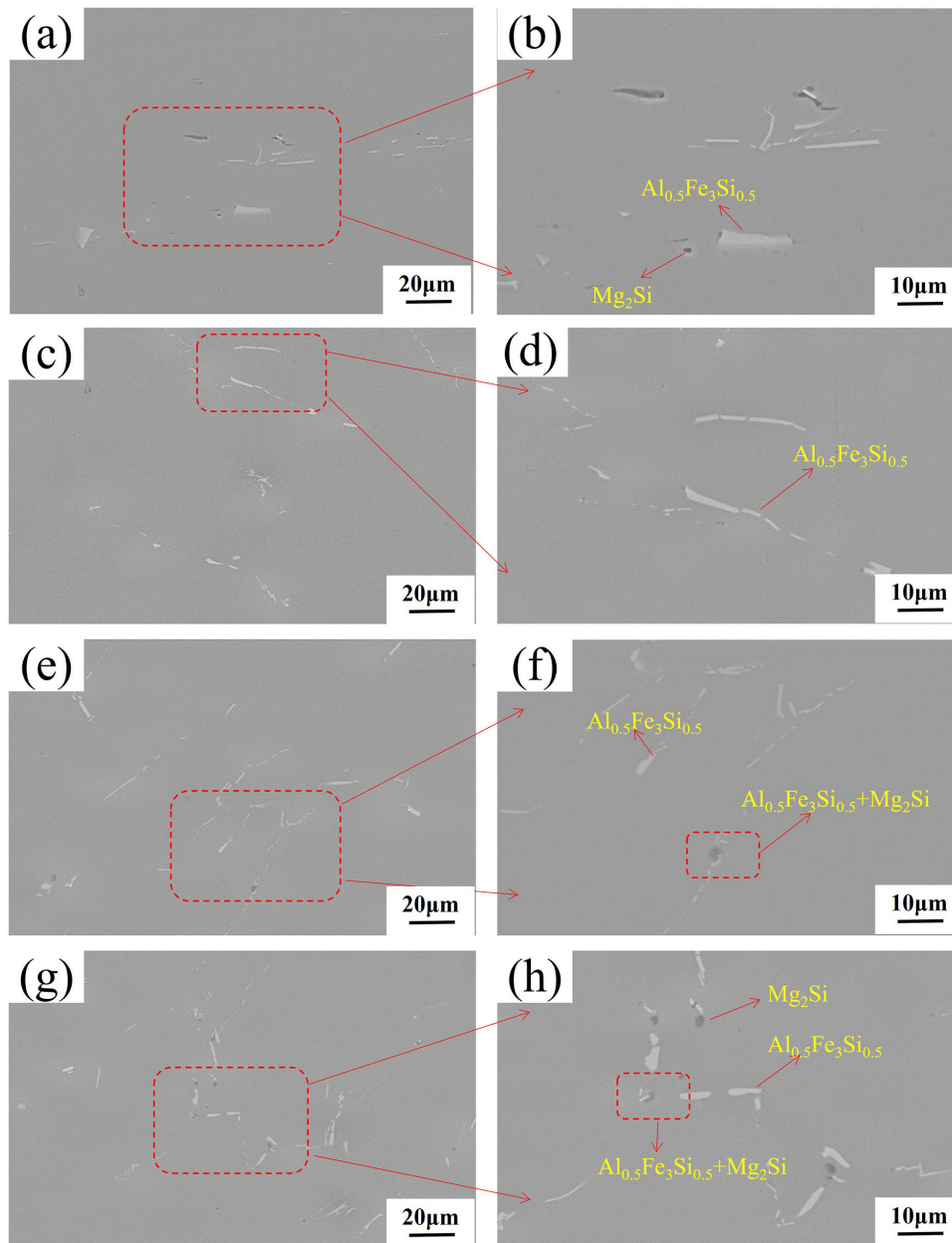


Figure 9: SEM images of the alloys in N zone at different states. As cast (a) and (b), 9 passes (c) and (d), solution treatment (e) and (f), aging (g) and (h).

3.5. The effect of MDF on mechanical properties and conductivity

Figure 10 shows the mechanical properties and engineering stress-strain curves of the alloys in N zone at different states. The UTS and YS of the as-cast alloy are 165 and 80 MPa, respectively. With the increase of forging passes, the mechanical properties of the alloy gradually increase. When the forging passes increase to 9, the UTS and YS increase to 223 and 136 MPa. Generally, the increase of strength is usually accompanied by the decrease of EL. However, the EL of the sample in this experiment is increased during the MDF, as shown in Figure 10b, 49.5% higher than that of the as-cast alloy. The reason is the coupling effect of deformation and grain refinement. After solution treatment, the UTS increases to 240 MPa upon the re-dissolution of second phases, which increases the driving force of aging precipitation and leads to more precipitates. Combined with Figure 9g and h, a large number of spheroidized, fine and dispersed second phases (Mg_2Si) precipitates, representing smaller surface energy and better strengthening effect. At the same time, aging treatment improves the inhomogeneity of grain size, reduces the residual stress, and improves the EL [30].

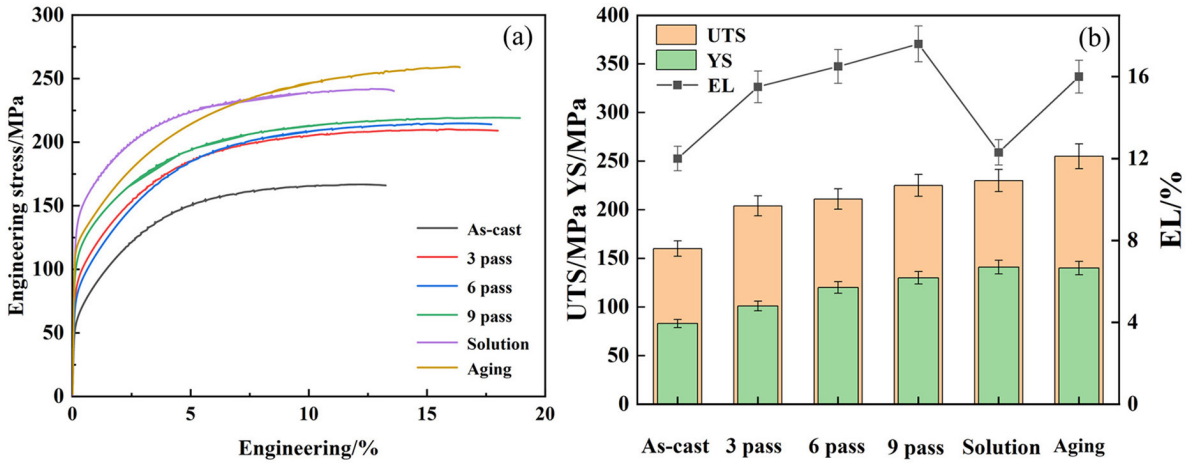


Figure 10: Engineering stress-strain curves (a) and mechanical properties (b) of the alloys in N zone at different states.

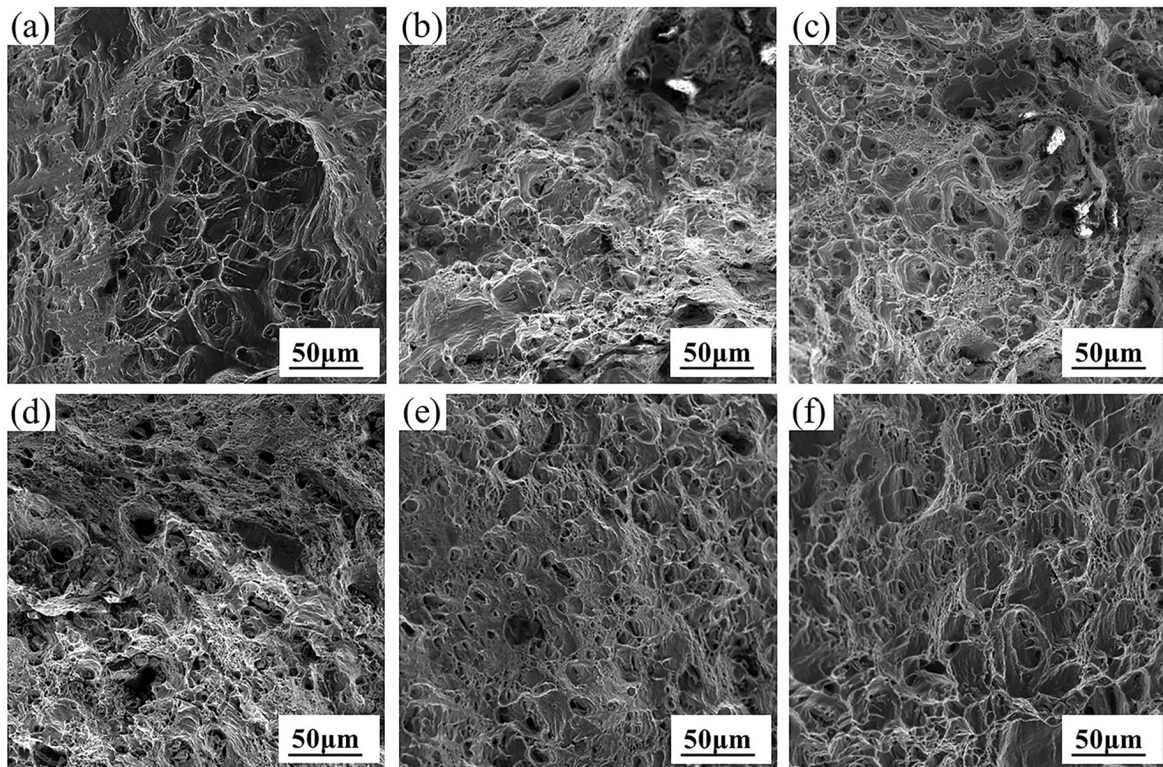


Figure 11: Tensile fractures of the alloys in N zone at different states. As cast (a), 3 passes (b), 6 passes (c), 9 passes (d), solution treatment (e) and aging (f).

Figure 11 shows the tensile fractures of the alloys in N zone at different MDF passes. As shown in Figure 11a, the fracture is characterized by the large and shallow dimples and the cleavage platform in as-cast aluminum alloy. However, after 3 passes of MDF, the cleavage plane gradually disappears, and the tearing edges appear. Some small dimples indicate that the plasticity is improved. From Figure 11c and d, the number of dimples gradually increases. At 9 passes, as shown in Figure 11d, the dimples are small and deep. The fracture is characterized by transgranular fracture, and part of the fracture is caused by the second phase particles. The fracture of solution treated alloy is shown in Figure 11e, the obvious cleavage plane appears, the number of dimples also decreases significantly, indicating the worse plasticity. As shown in Figure 11f, aging induces the smaller and deeper dimples, consistent with the higher EL of the alloy.

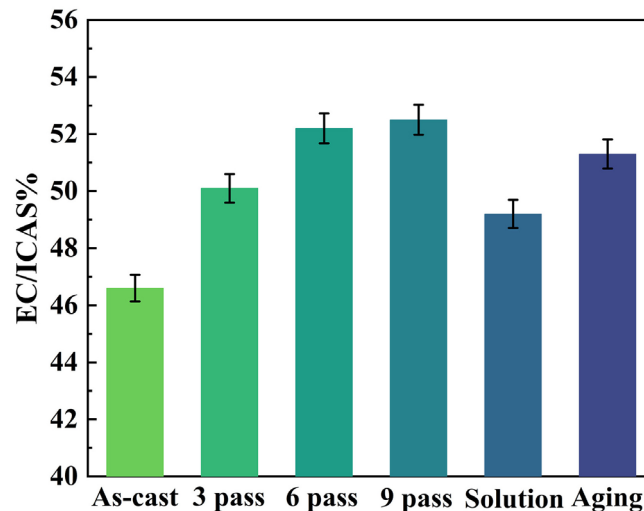


Figure 12: Electrical conductivity of the alloys in N zone at different states.

Figure 12 shows the electrical conductivity of the alloys in N zone at different states. The conductivity of the alloys at 3 and 6 passes is 50% IACS and 52.1% IACS, respectively. With the increase of forging passes, the conductivity increases to 52.8% IACS after 9 passes of MDF, 13.5% higher than that of the as-cast alloy. Since the higher the degree of solid solution of the alloy, the greater the degree of lattice distortion, the more serious the electron scattering. After solution treatment, the conductivity decreases to 49.1% IACS. The increase in conductivity of the alloy after aging can be explained as a result of the precipitation behavior of solid solution atoms. Mg_2Si precipitate in the alloy after aging causes the lower concentration of solute in the alloy, the reduced lattice distortion and the electron scattering. Therefore, the conductivity of the alloy is improved [31].

4. CONCLUSION

This work investigates the effects of MDF and heat treatment on the microstructure and properties of 6201 aluminum alloy. The evolution of alloy microstructure during MDF and heat treatment processes has been discussed. The changes in the mechanical and electrical properties of 6201 aluminum alloy have been analyzed. The conclusions are as follows:

- (1) In the process of MDF, the deformation of the alloy is not uniform. The inhomogeneity can be effectively improved with the increase of forging passes. With the increase of forging passes, the structure of the alloy tend to be consistent, and the grains are effectively refined.
- (2) The size of the second phase decreases during the MDF process, and with the increase of forging passes, the second phase is broken and reduced. The size of Mg_2Si phase is reduced to 2-3 μm , and some of them dissolve in the matrix.
- (3) Fine grain strengthening and second phase strengthening are the main factors in improving the mechanical properties of alloys. With the increase of forging passes, the mechanical properties of the alloy are improved. After heat treatment, the UTS and conductivity reaches 257 MPa and 51.6% IACS, respectively.

5. ACKNOWLEDGMENTS

This work was supported by the National Key Research and Development Program of China [grant No. 2022YFE0137900, 2022YFB3706801], Dalian High-level Talents Innovation Support Program [grant No. 2021RD06], National Natural Science Foundation of China [grant No. U2341253, 52371019, U2241232], Applied Basic Research Program of Liaoning Province [grant No. 2022JH2/101300003], and Natural Science Foundation of Liaoning Province [grant No. 2022-BS-262, JYTMS20230031].

6. BIBLIOGRAPHY

- [1] YAMANE, T., KONDOU, R., MAKABE, C., "Grain refinement and strengthening of a cylindrical pure-aluminum specimen by using modified equal-channel angular pressing technique", *Key Engineering Materials*, v. 340–341, pp. 937–942, 2007. doi: <http://dx.doi.org/10.4028/www.scientific.net/KEM.340-341.937>.

- [2] TORRES, L.V., ZOQUI, E.J., “Realization of the innovative potential of radial-shear rolling for forming the structure and mechanical properties of AISI-321 austenitic stainless steel”, *Matéria*, v. 25, n. 2, 2020. doi: <http://dx.doi.org/10.1590/s1517-707620200002.1028>.
- [3] CARDOSO, K., GUIDO, V., SILVA, G., *et al.*, “Microstructural evolution of AA7050 al alloy processed by ECAP”, *Matéria*, v. 15, n. 2, pp. 291–298, 2010. doi: <http://dx.doi.org/10.1590/S1517-70762010000200029>.
- [4] LUKYANOV, A., CHURAKOVA, A., FILATOV, A., *et al.*, “Microstructure refinement in Cu-Fe alloy using high pressure torsion”, *IOP Conference Series. Materials Science and Engineering*, v. 63, n. 1, pp. 012102, 2014. doi: <http://dx.doi.org/10.1088/1757-899X/63/1/012102>.
- [5] ZHANG, C., LIANG, C., LIANG, T., *et al.*, “Enhanced mechanical properties of an Mg-Zn-Ca alloy via high pressure torsion and annealing for use in bone implantation”, *Matéria*, v. 27, n. 3, e20220005, 2022. doi: <http://dx.doi.org/10.1590/1517-7076-rmat-2022-0005>.
- [6] RICHERT, M., HUBICKI, R., LEBKOWSKI, P., “Perspectives of microstructure refinement of aluminum and its alloys by the reciprocating extrusion (Cyclic Extrusion Compression – CEC)”, *Materials*, v. 15, n. 11, pp. 4006, 2022. doi: <http://dx.doi.org/10.3390/ma15114006>. PubMed PMID: 35683304.
- [7] KARAMI, S., PIROOZI, B., BORHANI, E., “Fatigue-induced microstructure evolution and ratcheting behavior of ultrafine-grained (UFG) pure aluminum processed by accumulative roll bonding (ARB)”, *Materials Characterization*, v. 196, pp. 112578, 2023. doi: <http://dx.doi.org/10.1016/j.matchar.2022.112578>.
- [8] MANJUNATH, G.A., SHIVAKUMAR, S., AVADHANI, S.P., *et al.*, “Investigation of mechanical properties and microstructural behavior of 7050 aluminium alloy by multi directional forging technique”, *Materials Today: Proceedings*, v. 27, n. 2, pp. 1147–1151, 2020. doi: <http://dx.doi.org/10.1016/j.matpr.2020.02.001>.
- [9] ZHANG, Z.J., YUAN, L., ZHENG, M.Y., *et al.*, “Achievement of high strength and good ductility in the large-size AZ80 Mg alloy using a designed multi-directional forging process and aging treatment”, *Journal of Materials Processing Technology*, v. 311, pp. 117828, 2023. doi: <http://dx.doi.org/10.1016/j.jmatprotec.2022.117828>.
- [10] WANG, D., YI, Y.P., LI, C., *et al.*, “Effects of different multidirectional forging processes on the microstructure and three-dimensional mechanical properties of ultra-high strength aluminum alloys”, *Materials Science and Engineering A*, v. 826, pp. 141932, 2021. doi: <http://dx.doi.org/10.1016/j.msea.2021.141932>.
- [11] EBRAHIMI, R., SHAFIEI, E., “Mathematical modeling of single peak dynamic recrystallization flow stress curves in metallic alloys”, In: Sztwiernia, K. (ed), *Recrystallization*, London, InTech. doi: <http://dx.doi.org/10.5772/34445>.
- [12] SITDIKOV, O., SAKAI, T., GOLOBORODKO, A., *et al.*, “Grain refinement in coarse-grained 7475 Al alloy during severe hot forging”, *Philosophical Magazine*, v. 85, n. 11, pp. 1159–1175, 2005. doi: <http://dx.doi.org/10.1080/14786430412331325049>.
- [13] RAO, P.N., SINGH, D., JAYAGANTHAN, R., “Mechanical properties and microstructural evolution of Al 6061 alloy processed by multidirectional forging at liquid nitrogen temperature”, *Materials & Design*, v. 56, pp. 97–104, 2013. doi: <http://dx.doi.org/10.1016/j.matdes.2013.10.045>.
- [14] AOBA, T., KOBAYASHI, M., MIURA, H., *et al.*, “Microstructural evolution and enhanced mechanical properties by multi-directional forging and aging of 6000 series aluminum alloy”, *Materials Transactions*, v. 59, n. 3, pp. 373–379, 2018. doi: <http://dx.doi.org/10.2320/matertrans.L-M2017856>.
- [15] MIKHAYLOVSKAYA, A.V., KISHCHIK, M.S., KOTOV, A.D., *et al.*, “Grain refinement during isothermal multidirectional forging due to β -phase heterogenization in Al-Mg-based alloys”, *Materials Letters*, v. 321, pp. 132412, 2022. doi: <http://dx.doi.org/10.1016/j.matlet.2022.132412>.
- [16] MOGHANAKI, S.K., KAZEMINEZHAD, M., LOGÉ, R., “Heating rate effect on particle stimulated nucleation and grains structure during non-isothermal annealing of multi-directionally forged solution treated AA2024”, *Materials Characterization*, v. 127, pp. 317–324, 2017. doi: <http://dx.doi.org/10.1016/j.matchar.2017.03.025>.
- [17] WANG, M., HUANG, L.P., LIU, W.S., *et al.*, “Influence of cumulative strain on microstructure and mechanical properties of multi-directional forged 2A14 aluminum alloy”, *Materials Science and Engineering A*, v. 674, pp. 40–51, 2016. doi: <http://dx.doi.org/10.1016/j.msea.2016.07.072>.
- [18] KHOJASTEHNEZHAD, V.M., POURASL, H.H., “Microstructural characterization and mechanical properties of aluminum 6061-T6 plates welded with copper insert plate (Al/Cu/Al) using friction stir welding”, *Transactions of Nonferrous Metals Society of China*, v. 28, n. 3, pp. 415–426, 2018. doi: [http://dx.doi.org/10.1016/S1003-6326\(18\)64675-8](http://dx.doi.org/10.1016/S1003-6326(18)64675-8).

- [19] CHEN, J., YAN, W., LIU, C.X., *et al.*, “Dependence of texture evolution on initial orientation in drawn single crystal copper”, *Materials Characterization*, v. 62, n. 2, pp. 237–242, 2010. doi: <http://dx.doi.org/10.1016/j.matchar.2010.12.006>.
- [20] ABIOYE, T.E., ZUHAILAWATI, H., AIZAD, S., *et al.*, “Geometrical, microstructural and mechanical characterization of pulse laser welded thin sheet 5052-H32 aluminium alloy for aerospace applications”, *Transactions of Nonferrous Metals Society of China*, v. 29, n. 4, pp. 667–679, 2019. doi: [http://dx.doi.org/10.1016/S1003-6326\(19\)64977-0](http://dx.doi.org/10.1016/S1003-6326(19)64977-0).
- [21] MIAO, Y.G., ZHANG, B.S., WU, B.T., *et al.*, “Joint characteristics and corrosion properties of bypass-current double-sided arc-welded aluminum 6061 alloy with Al-Si filler metal”, *Acta Metallurgica Sinica*, v. 29, n. 4, pp. 360–366, 2016. doi: <http://dx.doi.org/10.1007/s40195-016-0394-1>.
- [22] SUÁREZ-PENÑA, B., ASENSIO-LOZANO, J., “Influence of Sr modification and Ti grain refinement on the morphology of Fe-rich precipitates in eutectic Al-Si die cast alloys”, *Scripta Materialia*, v. 54, n. 9, pp. 1543–1548, 2006. doi: <http://dx.doi.org/10.1016/j.scriptamat.2006.01.029>.
- [23] SCHMID, E.E., OLDENBURG, K., FROMMEYER, G., “Microstructure and properties of as-cast intermetallic Mg₂Si-Al alloys / microstructure and properties of as-cast intermetallic Mg₂Si-Al alloys”, *International Journal of Materials Research*, v. 81, n. 11, pp. 809–815, 1990. doi: <http://dx.doi.org/10.1515/ijmr-1990-811106>.
- [24] ZHANG, G.Z., WANG, C.F., YIN, S.Q., *et al.*, “Development of low-carbon energy storage material: electrochemical behavior and discharge properties of iron-bearing Al–Li-based alloys as Al–air battery anodes”, *Journal of Power Sources*, v. 585, pp. 233654, 2023. doi: <http://dx.doi.org/10.1016/j.jpowsour.2023.233654>.
- [25] SENKOV, O.N., FROES, F.H., STOLYAROV, V.V., *et al.*, “Microstructure and microhardness of an Al Fe alloy subjected to severe plastic deformation and aging”, *Nanostructured Materials*, v. 10, n. 5, pp. 691–698, 1998. doi: [http://dx.doi.org/10.1016/S0965-9773\(98\)00107-X](http://dx.doi.org/10.1016/S0965-9773(98)00107-X).
- [26] HEWITT, P., BUTLER, E.P., “Mechanisms and kinetics of θ' dissolution in Al-3% Cu”, *Acta Metallurgica*, v. 34, n. 7, pp. 1163–1172, 1986. doi: [http://dx.doi.org/10.1016/0001-6160\(86\)90002-7](http://dx.doi.org/10.1016/0001-6160(86)90002-7).
- [27] FÁTAY, D., BASTARASH, E., NYILAS, K., *et al.*, “X-ray diffraction study on the microstructure of an Al-Mg-Sc-Zr alloy deformed by high-pressure torsion”, *International Journal of Materials Research*, v. 94, n. 7, pp. 842–847, 2003. doi: <http://dx.doi.org/10.3139/IJMR-2003-0148>.
- [28] COWDERY, S.J., KAYSER, F.X., “Lattice parameters of ferromagnetic DO₃-structured iron-aluminum-silicon alloys”, *Materials Research Bulletin*, v. 14, n. 1, pp. 91–99, 1979. doi: [http://dx.doi.org/10.1016/0025-5408\(79\)90236-8](http://dx.doi.org/10.1016/0025-5408(79)90236-8).
- [29] GU, C.Y., ZHANG, G.Z., JIN, H.M., *et al.*, “Research of rolling-drawing coupled deformation on the microstructure-property evolution and strengthening mechanism of 6201 conductive tubes”, *Journal of Materials Research and Technology*, v. 18, pp. 3933–3948, 2022. doi: <http://dx.doi.org/10.1016/j.jmrt.2022.04.085>.
- [30] DINIZ, S.B., PAULA, A.S., BRANDÃO, L.P., “Temperature and annealing time influences on cross-rolled 7475-T7351 aluminum alloy”, *Matéria*, v. 27, n. 4, e20220167, 2022. doi: <http://dx.doi.org/10.1590/1517-7076-rmat-2022-0167>.
- [31] CHO, C.H., CHO, H., “Effect of dislocation characteristics on electrical conductivity and mechanical properties of AA 6201 wires”, *Materials Science and Engineering A*, v. 809, pp. 140811, 2021. doi: <http://dx.doi.org/10.1016/j.msea.2021.140811>.